Journal of Quantitative Spectroscopy & Radiative Transfer 277 (2022) 107951

Contents lists available at ScienceDirect

Journal of Quantitative Spectroscopy & Radiative Transfer

journal homepage: www.elsevier.com/locate/jqsrt

Collisional line-shape effects in accurate He-perturbed H_2 spectra

Michał Słowiński[a,*], Hubert Jóźwiak[a], Maciej Gancewski[a], Kamil Stankiewicz[a], Nikodem Stolarczyk[a], Yan Tan[b], Jin Wang[b], An-Wen Liu[b], Shui-Ming Hu[b], Samir Kassi[c], Alain Campargue[c], Konrad Patkowski[d], Piotr S. Żuchowski[a], Roman Ciuryło[a], Franck Thibault[e], Piotr Wcisło[a]

[a] Institute of Physics, Faculty of Physics, Astronomy and Informatics, Nicolaus Copernicus University in Toruń, Grudziadzka 5, Torun 87-100, Poland
[b] Hefei National Laboratory for Physical Sciences at Microscale, iChEM, University of Science and Technology of China, Hefei, 230026 China
[c] University of Grenoble Alpes, CNRS, LIPhy, Grenoble F-38000, France
[d] Department of Chemistry and Biochemistry, Auburn University, Auburn, AL 36849 USA
[e] Univ Rennes, CNRS, IPR (Institut de Physique de Rennes) - UMR 6251, Rennes F-35000, France

ARTICLE INFO

Article history:
Received 26 March 2021
Revised 21 September 2021
Accepted 21 September 2021
Available online 23 September 2021

Keywords:
ab initio quantum-scattering Calculations
Molecular hydrogen
Spectral line shape
Collisional line-shape effects

ABSTRACT

We investigate collisional line-shape effects that are present in highly accurate experimental spectra of the 3-0 S(1) and 2-0 Q(1) molecular hydrogen absorption lines perturbed by helium. We clearly distinguish the influence of six different collisional effects (i.e.: collisional broadening and shift, their speed dependencies and the complex Dicke effect) on the shapes of H_2 lines. We demonstrate that only a very specific combination of these six contributions, determined from our *ab initio* calculations, gives unprecedentedly good agreement with experimental spectra. If any of the six contributions is neglected, then the experiment-theory comparison deteriorates at least several times. We also analyze the influence of the centrifugal distortion on our *ab initio* calculations and we demonstrate that the inclusion of this effect slightly improves the agreement with the experimental spectra.

1. Introduction

Hydrogen molecule, which is the simplest neutral chemically bound system, colliding with a helium atom constitutes a benchmark system well suited for testing and validating [1] the *ab initio* quantum chemical calculations of potential energy surfaces (PESs) [2,3]. The way the collisional effects are manifested in rovibrational spectra is particularly interesting in the case of the H_2 molecule. Due to a large rotational constant [4] and the lack of low-temperature inelastic channels in H_2 scattering [5], the nontrivial beyond-Voigt collisional line-shape effects are atypically strong [6], which makes it a perfect system for testing the collision-induced line-shape effects together with the quantum-scattering calculations associated with them.

Recently, low-temperature experiments with coexpanded supersonic beams allowed to measure rotationally inelastic scattering of the HD molecule colliding with D_2 [7,8] and with He [9]. The influence of collisions of H_2 isotopologues or noble gas atoms with a hydrogen molecule on the shapes of the H_2 lines was studied in a wide temperature range, spanning from 20 to 1200 K [10–17]. In particular, the widths and shifts of the H_2 rovibrational lines affected by the H_2-He collisions were subjected to intense theoretical and experimental studies [3,5,15,18–26]. Recently, the *ab initio* calculations carried out for two rovibrational lines of molecular hydrogen achieved a subpercent agreement with experimental spectra [1].

In this work, we investigate the shapes of two molecular hydrogen absorption lines perturbed by helium. We clearly distinguish the influence of six different collisional effects (i.e.: collisional broadening and shift, speed dependence of the broadening and the shift, and real and imaginary Dicke effect) on the shapes of H_2 lines. We demonstrate that only a specific combination of these six contributions, as resulting from our *ab initio* calculations, gives unprecedentedly good agreement with experimental spectra (0.87% for the 3-0 S(1) line and 0.33% for the 2-0 Q(1) line). Additionally, we extend the previous analysis [1] by introducing into our quantum-scattering calculations the impact of the centrifugal distortion (CD) on the H_2-He interaction. We note that the CD is

* Corresponding author.
E-mail addresses: mslowinski@umk.pl (M. Słowiński), piotr.wcislo@umk.pl (P. Wcisło).

https://doi.org/10.1016/j.jqsrt.2021.107951

introduced into our quantum-scattering calculations in a twofold manner. First, CD influences the calculations of the structure of the H_2 molecule, i.e. the energies of the rovibrational levels. This effect was already taken into account in all our previous analyses of the He-perturbed hydrogen lines [1,3,5,21–23,26]. In fact, we used the energy levels of H_2 reported in Ref. [27]. Second, CD influences the H_2-He interaction calculated from the PES for a given rovibrational state of H_2. This is because as the H_2 molecule rotates, its rovibrational wave function, $\chi_{vj}(r_{\mathrm{HH}})$, is slightly stretched. Thus, the full H_2-He PES should be averaged over wave functions which include this stretching (see Section 4 for details). In this paper, while referring to CD, we refer to the second meaning of those stated above. In the previous works it was pointed out that CD can be crucial for purely rotational lines [5]. Here, we demonstrate that while for the 2-0 Q(1) line, CD does not impact the line-shape parameters significantly, it influences the line-shape parameters of the 3-0 S(1) line at the 6% level and, hence, cannot be neglected in the interpretation of highly accurate experimental spectra.

Besides its importance for studying molecular interactions and collisions, accurate determination of the collisional line-shape parameters is important for astrophysical research. Spectroscopic studies of the atmospheres of giant planets need an accurate determination of pressure broadening and shift for electric-quadrupole H_2 lines [28–31]. Higher H_2 overtones are also used to study the atmospheres of giant planets [32,33], where beyond-Voigt line-shape parameters were proven to be necessary to interpret the measured spectra.

2. Line shape description

Our line-shape calculations [1,34–37] are based on the generalized Hess method (GHM) [38–40]. Instead of fitting, we calculate the line-shape parameters, namely the speed-dependent pressure broadening, $\Gamma(\nu)$, and shift, $\Delta(\nu)$ [41–43], along with the complex Dicke parameter, ν_{opt} [3,44–48], directly from the generalized spectroscopic cross sections

$$\Gamma(\nu)+i\Delta(\nu)=\left(\frac{n_p}{2\pi c}\right)\frac{2\tilde{v}_p^2}{\nu\sqrt{\pi}}\exp\left(-\nu^2/\tilde{v}_p^2\right)\times \times\int_0^\infty x^2e^{-x^2}\sinh\left(2\nu x/\tilde{v}_p\right)\sigma_0^q(x\tilde{v}_p)\mathrm{d}x, \tag{1a}$$

$$\nu_{\mathrm{opt}}=\left(\frac{n_p}{2\pi c}\right)\frac{m_p}{m+m_p}\int_0^\infty v_r f_m(v_r)\times \times\left[\frac{2}{3}\frac{v_r^2}{\overline{v}_r^2}\sigma_1^q(v_r)-\sigma_0^q(v_r)\right]\mathrm{d}v_r, \tag{1b}$$

where n_p is the number density of the perturber, c is the speed of light, v_p, v and v_r are the speed of the perturber with the most probable value $\tilde{v}_p$, the speed of the active molecule and their relative speed with mean value $\overline{v}_r$, respectively, with $x=v_r/\tilde{v}_p$. m_p and m are the masses of the perturber and the active molecule, respectively, and $f_m(v)$ is the Maxwell-Boltzmann speed distribution. The cross sections, $\sigma_\epsilon^q(v)$, are determined from the S-matrices that are obtained, from the binary impact approximation, from the quantum-scattering calculations [22], which are performed on the state-of-the-art H_2-He PES, i.e. extended Bakr, Smith and Patkowski potential (BSP3) [2,3]. The q superscript denotes the tensorial rank of radiation-matter interaction, which describes the type of a spectroscopic transition. In absorption spectroscopy, $q=1$ corresponds to electric dipole transitions and $q=2$ corresponds to the electric quadrupole transitions considered here. In the case of Raman spectroscopy, $q=0$ describes isotropic Q lines, while $q=2$ corresponds to anisotropic transitions. ϵ denotes the rank of the velocity tensor. For $\epsilon=0$, the real and imaginary part of $\sigma_\epsilon^q(v)$ are referred to as the pressure broadening and pressure shift cross sections, respectively [49–51], which describe the damping and dephasing of the optical coherence. For $\epsilon=1$ the $\sigma_\epsilon^q(v)$ provides the complex Dicke cross section [39,40,52], the real part of which describes the flow of the optical coherence between different velocity classes. The imaginary part of $\sigma_{\epsilon=1}^q(v)$ describes the phase changing of the optical coherence during velocity-changing collisions. We note that the cross sections, $\sigma_\epsilon^q(v)$, include the contribution from the inelastic scattering of the diatomic molecule and the dephasing part, which involves both the reorienting collisions (induced by the anisotropic part of the PES) and purely phase-changing collisions [5].

The isolated absorption line can be described in terms of the transport-relaxation equation [53]

$$1=-i(\omega-\omega_0-\mathbf{k}\cdot\mathbf{v})h(\omega,\mathbf{v})-\hat{S}^{\mathrm{f}}h(\omega,\mathbf{v}), \tag{2}$$

where ω and ω_0 are the laser frequency and the unperturbed line position, respectively, $\mathbf{k}$ is the wave vector, $\hat{S}^{\mathrm{f}}$ is the collision operator, $f_{\mathrm{m}}(\mathbf{v})$ is the Maxwell velocity distribution of the active molecule velocity, $\mathbf{v}$, and $f_{\mathrm{m}}(\mathbf{v})h(\omega,\mathbf{v})$ is a scalar function proportional to the velocity distribution of the optical coherence. The shape of molecular line is calculated as [53]

$$I(\omega)=\frac{1}{\pi}\Re e\int \mathrm{d}^3\mathbf{v}\; f_{\mathrm{m}}(\mathbf{v})h(\omega,\mathbf{v}). \tag{3}$$

The velocity distribution of the optical coherence arises as an interplay between two competing processes. On one hand, the laser light induces the optical excitation within some velocity classes. On the other, collisions change both the internal state of the molecule and its velocity [54–56]. These effects can be incorporated into the collision operator as a sum of the broadening and shift and a velocity-changing operator

$$\hat{S}^{\mathrm{f}}=-(\Gamma_0+i\Delta_0)-\left(\Gamma_{\mathrm{SD}}b_\gamma(v)+i\Delta_{\mathrm{SD}}b_\delta(v)\right)+ +(\nu_{\mathrm{opt}}^{\mathrm{r}}+i\nu_{\mathrm{opt}}^{\mathrm{i}})\hat{M}_\xi^{\mathrm{f}}, \tag{4}$$

where Γ_0 and Δ_0 are the speed-averaged broadening and shift, Γ_{SD} and Δ_{SD} are the parameters describing the magnitude of the speed-dependence of broadening and shift of the line with b_γ and b_δ describing their shape [35], ν_{opt}^r and ν_{opt}^i are the real and imaginary part of ν_{opt}, respectively. Finally, $\nu_{\mathrm{opt}}\hat{M}_\xi^{\mathrm{f}}$ is the velocity-changing operator [53,57,58] within a given ξ model of collisions

$$\nu_{\mathrm{opt}}\hat{M}_\xi^{\mathrm{f}}h(\omega,\mathbf{v})=\int\left[f_\xi(\mathbf{v}\leftarrow\mathbf{v}')-f_\xi(\mathbf{v}'\leftarrow\mathbf{v})\right]h(\omega,\mathbf{v}')\mathrm{d}\mathbf{v}', \tag{5}$$

where f_ξ is the collision kernel. We note here that the complex Dicke parameter, ν_{opt}, involves correlation between the internal and translational degrees of freedom [3,39,40,45]. In the original formulation of the GHM, this operator is a simple hard-collision (HC) operator [44,59] whose collision kernel depends only on the Maxwell velocity distribution [60]

$$f_{\mathrm{HC}}(\mathbf{v}\leftarrow\mathbf{v}')=\nu_{\mathrm{opt}}f_{\mathrm{m}}(\mathbf{v}). \tag{6}$$

In this work, we replace the HC collision kernel with the more physically-justified billiard-ball (BB) model [54,57,58], in which the collision kernel takes into account not only the speed after the collision, v, but also the speed before the collision, v', the angle ϕ between aforementioned velocities and the perturber-absorber mass ratio, α. The BB collision kernel can be expressed as

$$f_{\mathrm{BB}}(\mathbf{v}\leftarrow\mathbf{v}')= =\nu_{\mathrm{opt}}\frac{1}{v_{\mathrm{m}}^2}\frac{3}{32\pi}\frac{(1+\alpha)^{5/2}}{\alpha^2}\frac{1}{\sqrt{v^2-2vv'\cos(\phi)+v'^2}}\times \times\exp\left(-\frac{(1-\alpha)^2}{4\alpha}\frac{v'^2}{v_{\mathrm{m}}^2}-\frac{(1+\alpha)(1-\alpha)}{2\alpha}\frac{vv'}{v_{\mathrm{m}}^2}\cos(\phi)+\right.$$

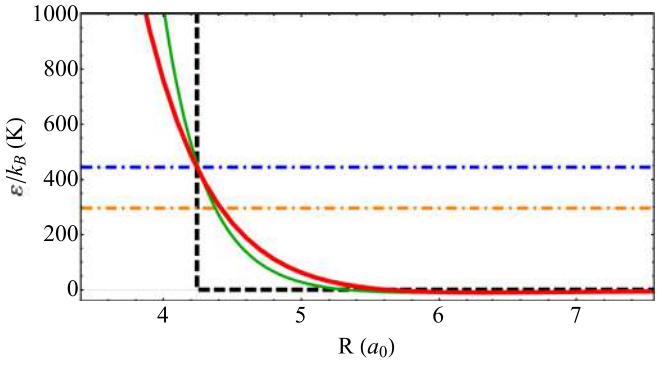

Fig. 1. Isotropic part of the BSP3 PES for colliding H_2-He (red thick solid line) as a function of relative distance, *R*. The hard-sphere potential (black dashed line) was constructed so it intersects the *ab initio* potential curve at the mean collisional energy (ε/k_B=444 K). Green solid line is the Lennard-Jones potential fitted to the isotropic part of the BSP3 PES. Mean collision energy and energy corresponding to the temperature *T* are indicated as the blue (upper) and orange (lower) dot-dashed lines respectively. The mean hard-sphere diameter $d_{H_2-He} = 4.24$ a$_0$ at 296 K.

$$+ \quad \frac{\alpha v^2 v'^2 \sin^2(\phi)}{v_m^2\left(v^2 - 2vv'\cos(\phi) + v'^2\right)} - \frac{(1+\alpha)^2}{4\alpha}\frac{v^2}{v_m^2}\Bigg), \tag{7}$$

where $v_m = \sqrt{2k_BT/m}$ is the most probable speed of an active molecule of mass *m*, k_B is the Boltzmann constant, and *T* is the temperature. With the BB model of collisions included, we refer to the line shape as the speed-dependent billiard-ball profile (SDBBP).

In this work, we calculate the complex Dicke parameter from the *ab initio* calculations based on the GHM. It is interesting to compare it with the frequency of the velocity-changing collisions (real number), ν_{diff}, calculated from the diffusion [57,61]

$$\nu_{diff} = \frac{v_m^2}{2D}, \tag{8}$$

where *D* is the binary diffusion coefficient. The latter can be simply calculated using a crude hard-sphere model [34,57] or an effective Lennard-Jones (LJ) potential parameters [62]. It can be also determined experimentally [63]. We estimate the mean hard-sphere diameter (σ in Ref. [34]) as the intersection of the true isotropic part of the PES with the mean collisional energy, see black line in Fig. 1. The effective LJ potential was obtained by fitting its parameters to the true isotropic part on the interacting pair in the ground state, see green line in Fig. 1.

Note that while this work focuses on describing the line shape in a physically justified model, we also provide a comprehensive dataset of the line-shape parameters for this system for the quadratic speed-dependent hard-collision profile in a wide temperature range in Ref. [17].

3. Signatures of different collisional line-shape effects in experimental spectra

In this section, we use the experimental spectra reported in Ref. [1]. The He-perturbed 2-0 Q(1) H_2 line was measured in the Grenoble laboratory at temperature 294.2 K and at nine pressures from 0.07 to 1.05 atm and the He-perturbed 3-0 S(1) H_2 line was measured in the Hefei laboratory at temperature 296.6 K and at four pressures from 0.36 to 1.35 atm. The H_2-He mixing ratio is different for both experiments and for the 2-0 Q(1) line has a constant value of 4.9(1)% while for the 3-0 S(1) line spans between 10% and 33%. We perform fully quantum calculations of the line-shape parameters on the newly-developed BIGOS code [64], see Ref. [3,22] for detailed description of the methodology. Comparing to our previous work [1] we perform additional quantum-scattering calculations to check the influence of the CD (which

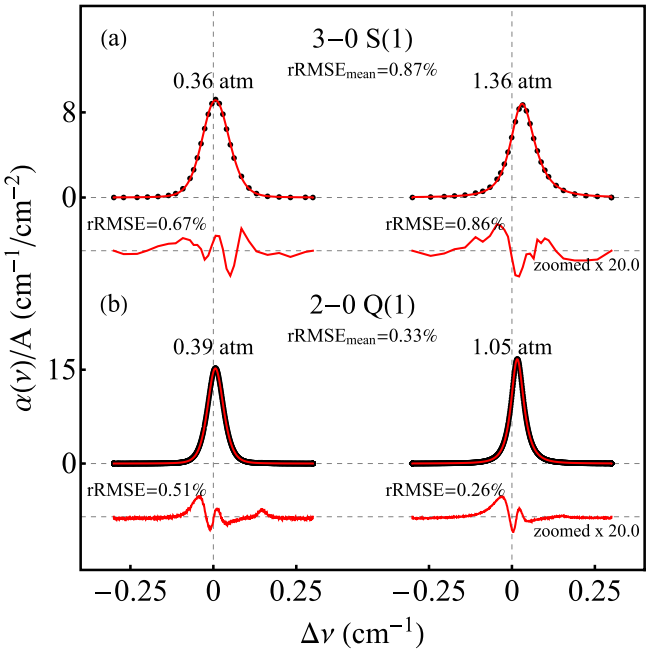

Fig. 2. The raw experimental spectra reported in Ref. [1] (black points) in comparison with the simulated line profiles (red lines). Linear background is subtracted from the spectra. The absorption axis is normalized to the spectral line area, *A*. The red lines under the line profiles show the differences between the experiment and theory enlarged twenty times. Relative root-mean-square error, rRMSE, values in the plots describe the errors relative to the profile amplitude calculated within ±FWHM (Full-Width at Half Maximum) from the line maximum. Vertical gray lines correspond to the theoretical unperturbed line position, ω_0. Deviation of the line maximum from ω_0 highlights that H_2 has atypically large pressure shift.

is usually neglected) on the shapes of molecular resonances, see Section 4 for more details. In our spectra analysis, we fit the line position, ω_0, line intensity, *S*, and linear baseline. The fit of the line position was performed by means of multispectrum fitting technique [65], while the line area was fitted separately for every pressure. Line-shape parameters are not fitted, but fixed to calculated *ab initio* values. The results for two chosen pressures are presented in Fig. 2. We have already demonstrated, in Ref. [1], that the consistency between our theoretical line-shape calculations and experimental data reaches subpercent accuracy for the He-perturbed H_2 lines. Here we demonstrate that taking into account more sophisticated line-shape parameters is crucial to achieve this agreement. In a typical case the collisional effects in molecular absorption spectra are dominated by the speed-averaged broadening, Γ_0, and shift, Δ_0, and hence the Voigt Profile (VP) suffices to describe the collision-perturbed shapes of the molecular lines [66,67]. However, the atypical properties of the hydrogen molecule give us an opportunity to experimentally study more subtle line-shape effects that our collision operator, Eq. (4), takes into account. In Sections 3.1–3.3 we demonstrate on the experimental data that none of these collisional effects can be neglected. Indeed, the excellent agreement between theory and experimental spectra, see Fig. 2, is achieved only when the contributions from all six collisional line-shape parameters are taken into account at the same time, see Fig. 3.

3.1. Speed-averaged line broadening and shift

The simplest description of the line shape is based on the speed-averaged broadening and shift in conjunction with the Doppler effect. In the absence of any other collisional line-shape effects, this results in the formation of a simple VP. To quantify the impact of these collisional effects on the overall shape of the

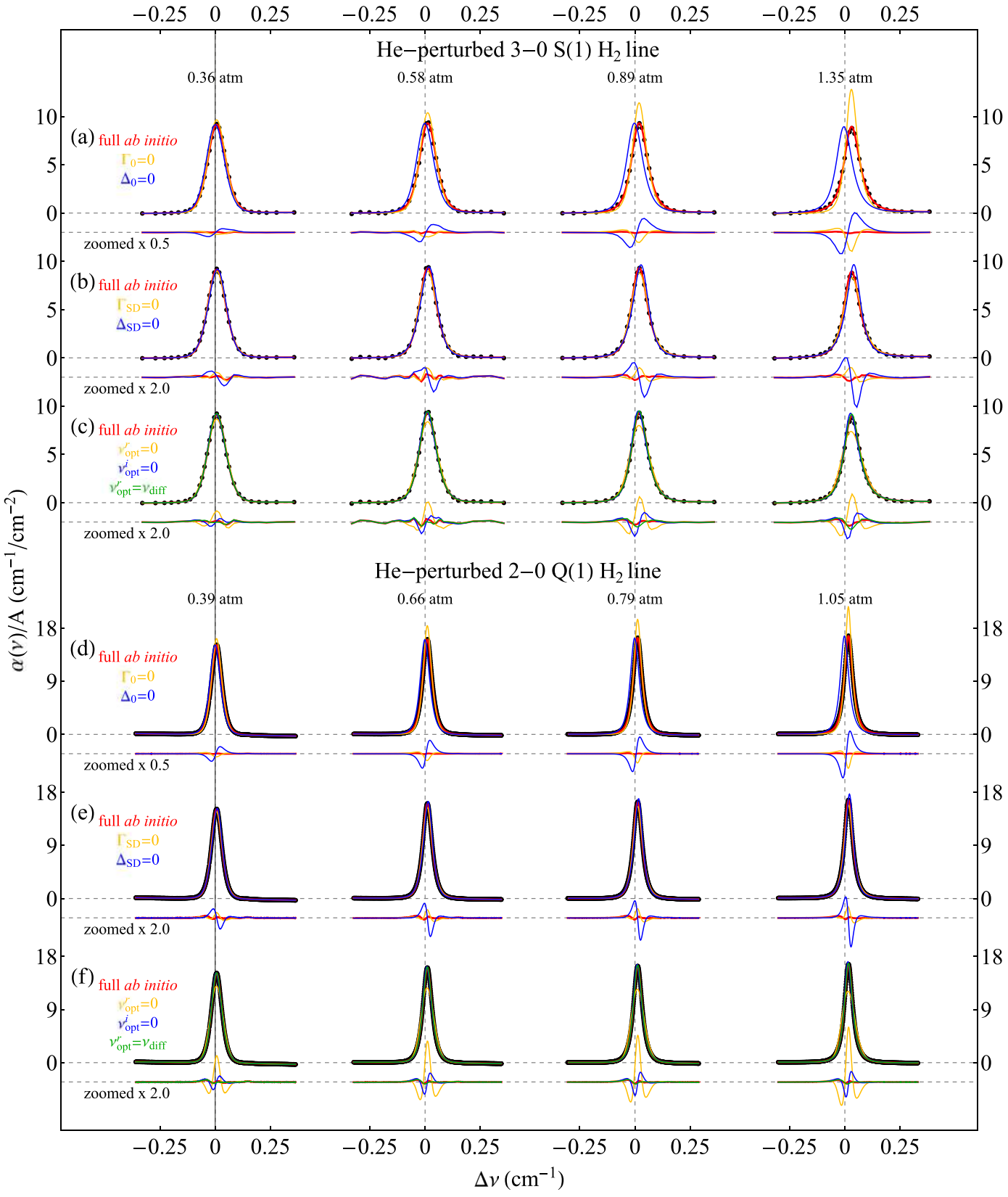

Fig. 3. Influence of different collisional effects on the shapes of the rovibrational transitions in H_2. Black dots are the experimental data reported in Ref. [1] and the red lines are the *ab initio* line shapes. Panels (a-c) and (d-f) correspond to the He-perturbed 3-0 S(1) and 2-0 Q(1) H_2 line, respectively. Panels (a) and (d) present the line shapes in which the speed-averaged line broadening and shift is neglected, i.e. $\Gamma_0 = 0$ (yellow line) and $\Delta_0 = 0$ (blue line). In panels (b) and (e) the speed dependence of the line broadening, $\Gamma_{SD} = 0$ (yellow line) and shift, $\Delta_{SD} = 0$ (blue line) is neglected. In panels (c) and (f) we neglect the complex Dicke parameter; its real, $\nu^r_{opt} = 0$ (yellow line), and imaginary, $\nu^i_{opt} = 0$ (blue line), parts. These panels also present the effect of replacing ν^r_{opt} with ν_{diff} originating from the diffusion model calculated with the hard-sphere approach (green line).

measured H_2 absorption lines, we set the Γ_0 (see yellow lines in Fig. 3a and d) and Δ_0 (see blue lines in Fig. 3a and d) parameters to zero in our *ab initio* profiles and directly superimpose them on the raw experimental data. The resulting large differences show, as expected, that both of these parameters are crucial for a proper description of the spectral profile.

3.2. Speed dependence of the line broadening and shift

For the present molecular system the simple VP is fairly insufficient [43,68,69]. The beyond-Voigt line-shape effects are particularly pronounced for the case of the rovibrational transitions in molecular hydrogen, see Fig. 2e–f in Ref. [1]. The dependence of the collisional width and shift on the speed of the molecules [41] has to be included to increase the agreement with experimental data. To examine its influence, we set the Γ_{SD} (see yellow lines in Fig. 3b and e) and Δ_{SD} (see blue lines in Fig. 3b and e) parameters to zero in our *ab initio* profiles and directly superimpose them on the raw experimental data. The speed dependence of the line width reduces the effective width of the line via the speed class exchanges, while the speed dependence of the shift manifests as inhomogeneous broadening and asymmetry of the line [70,71]. This is clearly confirmed by our experimental data, for $\Gamma_{SD} = 0$ (see aforementioned yellow line) the line-shape profile is broader, i.e., the peak of the line is lower, while for $\Delta_{SD} = 0$ (blue line) the line is narrower, i.e. the line peak is higher, and the residuals are clearly asymmetric.

3.3. Velocity-changing collisions

The influence of the velocity-changing collisions is incredibly pronounced for the H_2 molecule. It is clearly visible while comparing the velocity-changing collisions frequency derived directly from the diffusion coefficient, ν_{diff}, to the speed-averaged width, Γ_0 (for the values refer to the Table 1). Therefore, even if the state/phase- and velocity-changing collisions are correlated, i.e. some fraction of the excited molecules undergoing the change of the velocity are damped, the effective rate of velocity-changing collisions, ν_{opt}, is still much larger than all the other collisional line-shape parameters, see Table 1. We bring this to the fore this in Fig. 3 c and f; the yellow lines show the case when the real part of the complex Dicke parameter, ν^r_{opt}, is neglected.

For the considered lines, the real part of the complex Dicke parameter, ν^r_{opt}, is close to the one calculated from diffusion coefficient either using a hard-sphere model or LJ potential parameters (see the Appendix B of Ref. [3]), see Eq. (8), Fig. 1 and Table 1. The green lines in Fig. 3 c and f correspond to the case when the *ab initio* calculated ν^r_{opt} was replaced with ν_{diff}. Using ν^r_{opt} we achieved lower residuals than with this approach, but the differences on the figure scale is almost negligible.

In this analysis we clearly observe in experimental spectra the contribution of the imaginary part of the complex Dicke parameter, ν^i_{opt}. It has to be emphasized that here we do not phenomenologically fit the ν^i_{opt} parameter to the experimental data (which was done before many times [43,69,72–75]), but we set it to the value determined from our fully *ab initio* calculations and make a direct comparison with the raw experimental spectra, see the red lines in Fig. 3. To see the contribution from the ν^i_{opt} parameter we set it to zero and compare with experimental spectra, see the blue lines in Fig. 3 c and f. It can be clearly seen that when the contribution of ν^i_{opt} is neglected, then the discrepancy between theory and experiment is a few times larger.

3.4. Other collisional line-shape effects

In this section, we discuss several other collisional line-shape effects which we do not observe in our spectra. We argue that these effects have negligible influence in the cases considered here.

3.4.1. Non-impact (collision duration) effects

To estimate the influence of the collision-duration effect, we use the results obtained for the Ar-perturbed HF lines [76]. The asymmetry parameter, b, for this system is at the level of 3×10^{-3}amg^{-1}. At our highest pressure this would correspond to 0.15% rRMSE, which is smaller than the rRMSE of the comparison between experiment and theory reported in this work. This estimation is conservative since the range of the H_2-He interaction is smaller than for HF-Ar and the corresponding collision-duration effects for H_2-He are expected to be smaller as well.

3.4.2. Line mixing

To estimate the influence of the line-mixing effect, we use the results obtained for the selfperturbed HD lines [77]. The line-mixing coefficient, y, for HD-HD is at the level of 2×10^{-3}amg^{-1} [77]. At our highest pressure this would correspond to 0.1% rRMSE. Also this estimation is conservative since the separation between the Q lines is much larger for H_2 compared to the HD lines from Ref. [77].

Table 1
Line-shape parameters for the 3-0 S(1) and 2-0 Q(1) H_2 lines, determined with our *ab initio* quantum-scattering calculations that include centrifugal distortion. The calculations are done for $T =$ 296.6 K for the 3-0 S(1) line and for $T = 294.2$ K for the 2-0 Q(1) line. As a reference, we calculated also ν_{diff} from Eq. (8) for the hard-sphere and LJ potentials (see Fig. 1). For the hard-sphere potential, $\nu_{diff} = 43.38$ and 43.19 for $T = 296.6$ K and 294.2 K, respectively. For the LJ potential, $\nu_{diff} = 38.67$ and 38.43 for these two temperatures, respectively. For the experimentally determined diffusion coefficient [63], $\nu_{diff} = 40.9$ and 41.15 for $T = 296.6$ K and 294.2 K, respectively. All the parameters are given in 10^{-3} cm^{-1} and are calculated for $n_p = 1$ amg. Abbreviations of the PESs are given in the text.

PES	Γ_0	Δ_0	Γ_{SD}	Δ_{SD}	ν^r_{opt}	ν^i_{opt}
3-0 S(1) Line						
mMR	6.51	23.38	2.87	8.92	40.99	−13.03
SK	14.59	33.03	7.01	14.25	36.53	−19.28
BSP	12.79	31.52	5.91	12.99	37.32	−18.29
BSP2	12.36	31.15	5.70	12.67	37.57	−17.94
BSP3	12.38	31.14	5.71	12.69	37.56	−17.96
2-0 Q(1) Line						
mMR	3.45	14.28	1.59	5.53	42.63	−7.98
SK	7.04	21.89	3.35	9.25	41.25	−12.62
BSP	5.85	19.58	2.73	8.15	41.59	−11.51
BSP2	5.74	19.36	2.68	7.99	41.66	−11.33
BSP3	5.75	19.36	2.68	8.00	41.65	−11.35

4. Improved accuracy of the *ab initio* calculations

The analysis presented in the previous sections is based on the most recent *ab initio* PES (BSP3) [3]. In Section 3, we demonstrated that the *ab initio* line-shape calculations based on the BSP3 PES agree well with the experimental data. In this section, we use our quantum-scattering and line-shape calculations to validate the PESs available in the literature [2,3,78–80] as well as to quantify the influence of the CD, which is usually neglected in the scattering calculations for rovibrational transitions. The calculations that include CD are performed on the most accurate BSP3 PES using the newly developed BIGOS code [64].

For the purpose of scattering calculations, the PES for the H_2-He system, $V(R, r_{HH}, \theta)$ is expanded over Legendre polynomi-

als [3,5,22]

$$V(R, r_{\mathrm{HH}}, \theta) = \sum_{\lambda=0,2,4,6} V_\lambda(R, r_{\mathrm{HH}}) P_\lambda(\cos\theta), \tag{9}$$

where R is the separation between the helium atom and the center of mass of H_2, r_{HH} is the distance between hydrogen atoms, and θ denotes the angle between R and r_{HH}. Radial coupling terms, which enter the coupled equations, are obtained from the rovibrational average of the $V_\lambda(R, r_{\mathrm{HH}})$ terms over the wave functions of the unperturbed H_2 molecule, $\chi_{vj}(r_{\mathrm{HH}})$,

$$V_{\lambda,vj,v'j'}(R) = \int \mathrm{d}r_{\mathrm{HH}} \chi_{vj}(r_{\mathrm{HH}}) V_\lambda(R, r_{\mathrm{HH}}) \chi_{v'j'}(r_{\mathrm{HH}}), \tag{10}$$

where v and j denote vibrational and rotational quantum numbers, respectively. In this work we neglect the vibrational coupling between molecular states, which means that we use only radial coupling terms with $v' = v$ in the scattering calculations. The non-diagonal vibrational couplings would be too expensive to include. Disregarding the CD, in turn, means that in each vibrational state the coupling terms can be approximated as $V_{\lambda,vj,vj'}(R) \approx V_{\lambda,v0,v0}(R)$.

4.1. H_2-He potential energy surfaces

We consider five different PESs: the PES of Schaefer and Köhler (SK PES) [78], the modified Muchnick-Russek PES (mMR) [79,80], the PES reported by Bakr, Smith and Patkowski (BSP) [2] and its two extensions: BSP2 and BSP3 [3].

The original PES of Schaefer and Köhler was based on the *ab initio* points reported in Ref. [81] with the configuration interaction techniques. The SK PES covered a relatively large range of absorber-perturber distance R, (1.6 – 11 a_0) and was calculated for five intramolecular distances r_{HH} between 0.9 and 2 a_0, with three of them (1.28, 1.449, 1.618 a_0) determined at a higher level of accuracy [78]. The SK PES was originally presented in the form of $V_\lambda(R, r_{\mathrm{HH}})$ values. We made use of the form published in Ref. [80].

The mMR PES was published as a modification of the *ab initio* potential of Muchnick and Russek [79]. The original MR PES covered a narrow range of r_{HH} near 1.4 a_0, but the analytic fit was expected to behave reasonably even up to 4 a_0. The modification of this PES (mMR) [80] was performed to fit to the more accurate *ab initio* values reported in Ref. [82], which were calculated with the complete fourth-order Møller-Plesset approximation.

The BSP PES (and its further extensions) was obtained using the coupled-cluster method with single, double and perturbative triple (CCSD(T)) excitations, taking also into account the contributions from the higher coupled-cluster excitations [2]. This PES was determined for ten values of r_{HH} in the range of $r_{\mathrm{HH}} \in [1.1, 1.75]$ a_0, which turned out to be insufficient for the accurate studies of processes involving vibrationally excited H_2 (see Section 2 of Ref. [5] for details). This problem was solved in the second version of this PES, BSP2, which extended the *ab initio* data points range to $r_{\mathrm{HH}} \in [0.65, 3.75]$ a_0. In the final extension of this potential, BSP3, an improved asymptotic behavior for the large values of R was introduced (for details see Section 2 of Ref. [3]). This PES (denoted as BSP3) was used in Ref. [1].

In Table 1, we report the *ab initio* values of the line-shape parameters for all the considered PESs. There are no fitted line-shape parameters because for the molecular hydrogen they can considerably deviate from the real ones due to a strong numerical correlation. For this reason, we adopt a methodology that is more adequate to study the collisional effects in H_2, i.e., instead of comparing the fitted values of the collisional line-shape parameters with theory, we directly compare the *ab initio* line shapes with experimental spectra and the RMSE of their difference gives us information about the agreement between the theory and experiment.

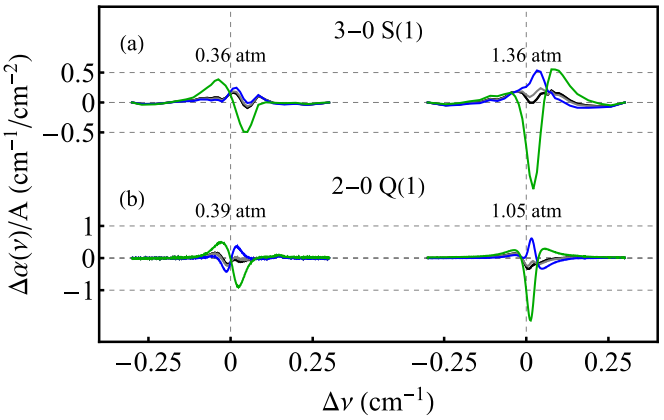

Fig. 4. Differences between experimental data and modelled spectra with central frequency fitted by means of the multispectrum fitting technique and line intensity fixed to the theoretical value [83]. Green, blue, gray and black lines are the residuals for the mMR, SK, BSP and BSP3 potentials, respectively. Vertical gray lines correspond to the unperturbed line position [83].

This way we can also check separately an individual influence of any of the six collisional line-shape parameters, see Fig. 3.

In Fig. 4 we show a comparison between the experiment and theory for different PESs. Contrary to the analysis from Figs. 2 and 3, here the line intensity is not adjusted but settled to the fixed theoretical value [83] (this is why the black residuals from Fig. 4 are slightly larger than the red ones from Figs. 2 and 3) to get a clear comparison and to not artificially compensate inaccurate values of some of the line-shape parameters by the line-fitting procedure.

The smallest residuals are for the most recent BSP3 PES, see the black lines in Fig. 4. The residuals for the BSP2 PES are hardly distinguishable from the ones for BSP3 (hence, we do not show them in Fig. 4). Physically, this means that any inaccuracies of the BSP2 potential at large separations between H_2 and He are minor relative to the sensitivity of the line-shape parameters to the asymptotic behavior of the PES, at this level of accuracy. This is consistent with the expectation that at room-temperature energies the generalized spectroscopic cross sections are hardly sensitive to the long-range part of the PESs (see Appendix C of Ref. [3]). The asymptotic behavior influences the values of the line-shape parameters at the subpercent level, see the BSP2 and BSP3 rows in Table 1.

The residuals for the BSP PES are shown in Fig. 4 as gray lines. The main difference between BSP and BSP3 is that BSP does not cover as large a range of intramolecular separations in H_2, see Fig. 1 in Ref. [5]. For the second overtone, at higher pressures, the residuals for BSP (blue line in the top panel in Fig. 4) are larger than for BSP3 (red line). It is consistent with our expectations but at the present level of accuracy the difference is not yet large enough to unambiguously conclude that we experimentally validate the highly-stretched regions of the PESs.

The residuals for the SK and mMR PESs are shown in Fig. 4 as blue and green lines, respectively. For these two cases, the residuals are much larger (especially for the mMR PES) than for the three versions of the BSP PES. This confirms the preliminary analysis of Ref. [5].

4.2. Centrifugal distortion (CD)

We performed additional scattering calculations on the BSP3 PES to determine the influence of the CD on the accuracy of theoretically modelled spectral line shapes. Figure 5 presents CD of the wave functions of H_2 in the three vibrational states considered in the experiment. The difference between the

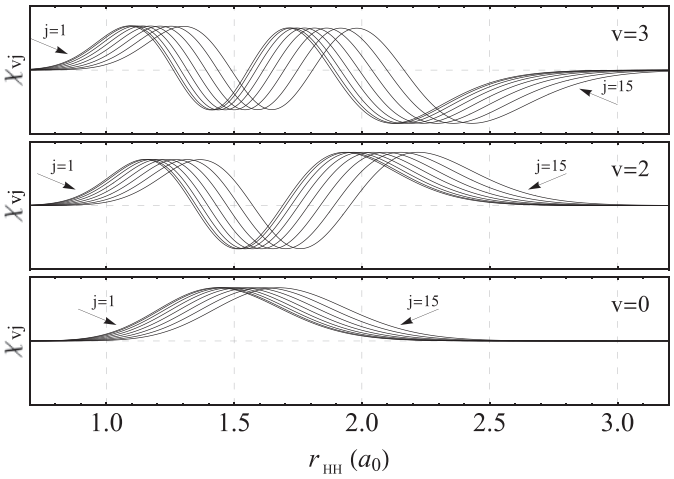

Fig. 5. Rovibrational wave functions of ortho-H_2, $\chi_{vj}(r_{HH})$ ($j = 1$ to $j = 15$) considered in our scattering calculations. For small j numbers the wave functions are overlapped.

purely vibrational state, $\chi_{v0}(r_{HH})$, and the true wave function, $\chi_{vj}(r_{HH})$, increases with both j and v. Due to the fact that H_2 has a remarkably large rotational constant ($B = 60.853$ cm^{-1} [4]), this effect should be pronounced in the rovibrational spectra of this molecule. The influence of the CD on the pressure broadening and shift coefficients was studied by Green [84] in the He-perturbed Q lines of D_2 from the fundamental band and by Shafer and Gordon [49] and Dubernet and Tuckey [85] in the He-perturbed isotropic Raman Q lines of the fundamental band and S purely rotational lines of H_2. These studies concluded that CD has a relatively small effect on both the pressure broadening and shift in the fundamental band (about 1–3%), but can significantly modify the pressure shift of the purely rotational lines, which is very sensitive to the difference in the elastic scattering in two rotational states. The majority of recent theoretical investigations [3,5,21–23] took this effect into account for purely rotational lines, but neglected it for rovibrational transitions. It was suggested [5] that in the latter case, CD might be masked due to the large contribution from the vibrational dephasing.

Here, we report values of the six line-shape parameters calculated with and without CD, see Table 2. In Fig. 6 we show the comparison between the experimental spectra and the theoretical line shape calculated with and without including the CD.

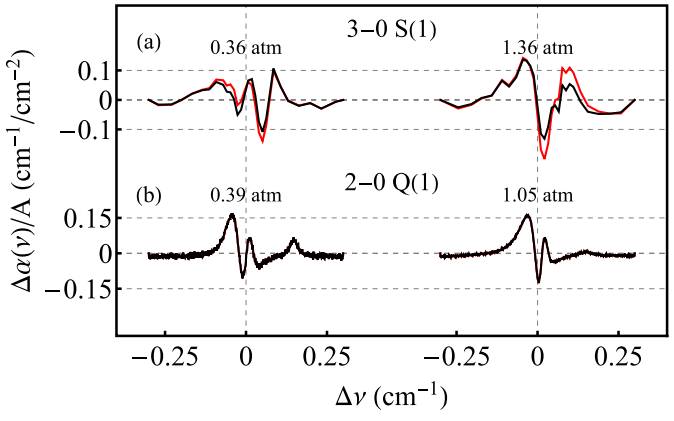

Fig. 6. The influence of centrifugal distortion (CD) on the theory-to-experiment consistency. We present differences between experimental data and modeled spectra with central frequency fitted by means of multispectrum fitting technique and line intensity fitted individually for each pressure. Black and red lines correspond to the cases when the CD was and was not taken into account, respectively. CD has a negligible effect on the Q line, therefore the lines are overlapping. Vertical gray lines correspond to the theoretical unperturbed line position.

For the 3-0 S(1) line, CD modifies the Γ_0 and Γ_{SD} by over 5%. The rest of the parameters, in particular, the pressure shift Δ_0, are modified by over 2.5%. CD leads to lower differences between theoretical and experimental spectra, and reduces the mean rRMSE calculated for ±FWHM from 0.99% to 0.89%. In the case of the 2-0 Q(1) line, CD has almost no effect on the calculated line-shape parameters and the spectra calculated with and without it overlap. This result agrees with the observation of Dubernet and Tuckey [85], who reported that the influence of CD on the Q(j) lines is significantly smaller than on the S(j) lines.

The fact that the collisional broadening for the two rovibrational lines which differ only in the final spectroscopic state differs by a factor of two might be surprising. As it turns out, collisional widths of rovibrational lines in H_2 (both He- and self-perturbed) exhibit an unusually strong dependence on the vibrational quantum number (see, for example Fig. 6 in Ref. [17] or Fig. 4 in Ref. [6]). This is caused by a large contribution to the line broadening from the vibrational dephasing, which mainly originates from the difference between the isotropic parts of the PES in initial and final vibrational states. As discussed in Refs. [3,5,22], this difference increases for 0-v transitions with v. Apart from the dephasing part, there is also a significant difference in the inelastic contribution to the collisional broadening between the $Q_v(1)$ and $S_v(1)$ lines. The former have significantly smaller inelastic contribution to Γ_0, due to the fact that the first inelastic transition from either initial or final spectroscopic state is possible once the first inelastic channel becomes accessible (here, for $E_{kin} \approx 500$cm^{-1}). On the other hand, for the $S_v(1)$ line the inelastic contribution from the scattering in the final spectroscopic state ($v, J = 3$) is non-zero even at very low kinetic energies. Moreover, the inelastic contribution increases with v because the spacing between the rotational energy levels in a given vibrational state decreases with v.

4.3. Propagation of the uncertainties of the line-shape parameters on the residuals

In the previous section, we demonstrate that an almost-6% change on the line-shape parameters can be introduced with the addition of the CD for the case of the 3-0 S(1) line, see Table 2. At the same time, in Fig. 2 we show that adding the CD improves the mean rRMSE for the 3-0 S(1) line by approximately 0.38% for the highest pressure (from 1.24% in Ref. [1] down to 0.86% in Fig. 2). In this section we explain this apparent inconsistency by analysing how the changes of the line-shape parameters propagate to the magnitude of the residuals. To do it, we directly simulate the line-shape profile for the original and corrected values of the line-shape parameters (the first and middle columns in Table 2, respectively) and we calculate rRMSE of the difference. All of the following discussion is made for the case of the 3-0 S(1) hydrogen line since CD, at this level of accuracy, has insignificant impact on the Q-branch lines [85].

The perturbations of Γ_0 and Δ_0 (by 5.65% and 2.06%, respectively) have the largest impact and change the profile by almost 2% for each of the two parameters in the high-pressure limit, see the top panel in Fig. 7. Curves overlapping with each other are a coincidence. For the case of our experiment, perturbations introduce an approximately 0.2% profile change (rRMSE) for the lowest and approximately 0.8% for the highest pressure. This is over 7 times less than the magnitude of the Γ_0 correction. As a reference for the numerical tests, we derive a simple analytical formula that describes propagation of the Γ_0 and Δ_0 uncertainties on the residuals for the case of the Lorentz Profile (LP), see Appendix A. The analytical values, which are valid in the high-pressure limit in which the profile is close to the LP, are shown in the top panel in

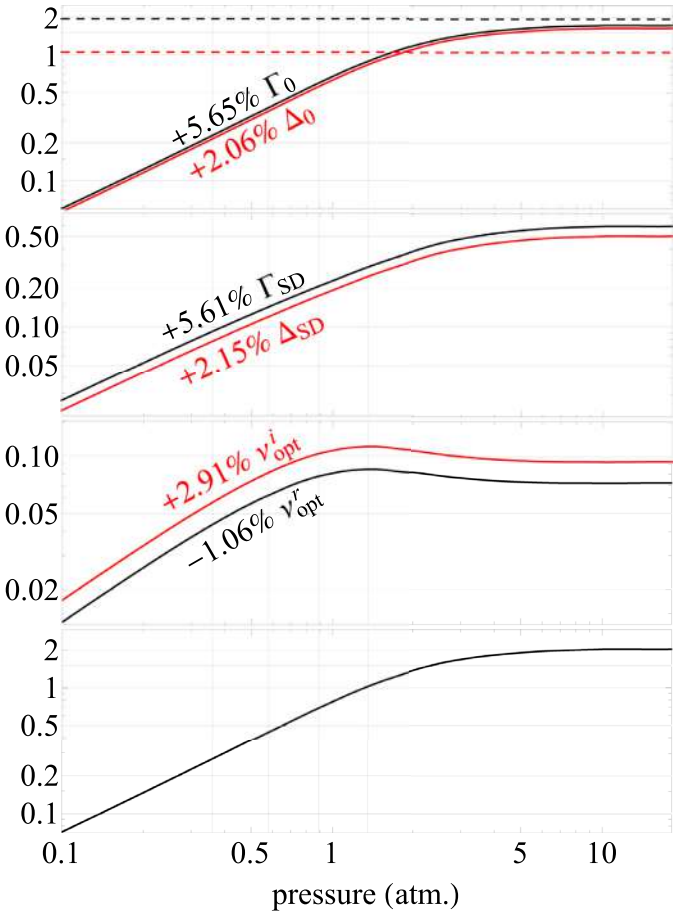

Fig. 7. Propagation of the uncertainties of the line-shape parameters on the residuals for the case of the He-perturbed 3-0 S(1) H_2 line. The vertical axis is rRMSE of the difference between the SDBBP generated for the uncorrected and centrifugal-distortion corrected values of the line-shape parameters (see Table 2). The first three panels show the results for the case when only one line-shape parameter is changed (see the labels in the plots). It is a coincidence that the two lines in the top panel overlap. The bottom panel shows the overall difference when all six line-shape parameters are changed. The dashed lines in the top panel are the analytical reference values (the same color notation as for solid lines), see Appendix A. The gray vertical lines correspond to the experimental pressures covered in this paper.

Table 2
Line-shape parameters for the 3-0 S(1) and 2-0 Q(1) H_2 lines, determined with our *ab initio* quantum-scattering calculations, using the BSP3 PES. Columns show the impact of the centrifugal distortion (CD) included in the calculations, showing both the line-shape parameter values and differences respective to the ones reported in Ref [1]. The calculations are done for $T = 296.6$ K for the 3-0 S(1) line and for $T = 294.2$ K for the 2-0 Q(1) line with the corresponding Doppler frequency equal to $\omega_D = 64.01 \times 10^{-3}$ cm^{-1} and 41.96×10^{-3} cm^{-1}, respectively. All the parameters are given in 10^{-3} cm^{-1} and are calculated for $n_p = 1$ amg.

		Ref. [1]	Ref. [1]+CD	Δ [%]
3-0 S(1) Line	Γ_0	11.72	12.38	5.65
	Δ_0	30.51	31.14	2.06
	Γ_{SD}	5.40	5.71	5.61
	Δ_{SD}	12.42	12.69	2.15
	ν^r_{opt}	37.96	37.56	−1.06
	ν^i_{opt}	−17.45	−17.96	2.91
2-0 Q(1) Line	Γ_0	5.74	5.75	0.17
	Δ_0	19.51	19.36	−0.77
	Γ_{SD}	2.68	2.68	0.00
	Δ_{SD}	8.06	8.00	−0.74
	ν^r_{opt}	41.64	41.65	0.02
	ν^i_{opt}	−11.31	−11.35	0.35

Fig. 7 as the dashed horizontal lines (black for Γ_0 and red for Δ_0). The full numerical values (solid lines in the top panel in Fig. 7) in the high-pressure limit are close to the analytical values. The slight difference is caused by the influence of the speed-dependent effects, the velocity-changing collisions, and the competition between them [70] that are present in our full line-shape model.

The perturbations of Γ_{SD} and Δ_{SD} have an approximately four-times smaller impact on the profile than the speed-averaged ones, with a maximum change of approximately 0.5% in the high-pressure limit and changes approximately 0.07% and 0.3% for lowest and highest experimental pressure, respectively, see the second panel in Fig. 7. The corrections of both ν^r_{opt} and ν^i_{opt} change the rRMSE by approximately 0.1% in the high-pressure limit and by approximately 0.05% and 0.1% for the low and high experimental pressures, respectively, see the third panel in Fig. 7. It is worth mentioning that for the differences introduced by the complex Dicke narrowing changes, the rRMSE curve has a different shape and has a maximum around 1.5 atm instead of an infinite pressure.

Introducing all corrections at once leads to an approximately 2% rRMSE change in the high-pressure limit, see the bottom panel in Fig. 7. For the case of our experiment, the changes are approximately 0.3% and 1% for the lowest and highest experimental pressure, which are impressively low taking into account the almost-6% magnitude of perturbations. The actual difference between residuals (from the theory-experiment comparison) for the cases with and without CD is even smaller than 0.3% and 1% for the lowest and highest experimental pressures. This is caused by the fact that the line intensity and linear baseline were fitted to the experimental data.

4.4. Relation of the present results with the previous works

It is true that the standard phenomenological models, taking into account the speed-dependent broadening and shift and complex Dicke-narrowing, with fitted parameters can provide a better representation of the data. Let us recall some recent works for the H_2 isotopologues. In Ref. [35] for a self-broadened D_2 line, it was shown that the SDBBP is able to fit experimental data within the experimental noise when all the parameters are adjusted. Fitting all the parameters leads to a significant improvement of the quality of the fit, however, some discrepancy between the parameters obtained from the fit and those from *ab initio* calculations was observed. In the case of the pressure broadening parameter it leads to a 14% deviation, while in the case of the parameter characterizing the speed dependence of the collisional width and shift, the deviation can even exceed an order of magnitude. Several D_2 lines from the same band were analyzed in Ref. [86] using the speed-dependent Nelkin-Ghatak profile (SDNGP) with a quadratic speed dependence of collisional broadening and shift. This profile was also able to fit the experimental data within the experimental noise when all the line-shape parameters were fitted. It should be pointed out, however, that the narrowing parameter obtained from the SDNGP fit differs by a factor of about 3 from the SDBBP fit. Also, SDNGP with a quadratic speed dependence of collisional broadening and shifting was applied to the H_2 lines in Ref. [35] and was able to fit experimental data within the experimental noise. The narrowing parameter obtained from this fit differs by a factor of 2 from the expected value and the speed dependence was overestimated (Γ_{SD} was larger than 2/3 Γ_0, which is unphysical). These examples as well as older works in literature considering H_2 lines clearly show that the phenomenological models can fit experimental data well, however, the physical meaning of the parameters is problematic. Therefore, in this work we are focused on a direct comparison of *ab initio* calculations and exper-

imental data rather than on fitting some phenomenological line-shape profiles.

We would like to emphasize that in the present work we performed an advanced analysis of the H_2 spectra that has not been done before. Our analysis provides a deep physical understanding of the collisional effects imprinted in the shapes of the H_2 lines. The key result of the present work is shown in Fig. 3. In contrast to the previous works, here we analyze step-by-step the contribution of each of the six collisional line-shape effects. For instance, the blue line in Fig. 3b shows that the very strong speed dependence of the collisional shift is essential for an accurate description of the spectra. Furthermore, in Fig. 3 we demonstrate the importance of the contribution of the imaginary part of the Dicke parameter. We show that if we set the imaginary part of the Dicke parameter to zero, then the agreement between theory and experiment is a few times worse. In Fig. 3, we also demonstrate that all of these six collisional contributions have to be taken into account to reach this high agreement with experiment. This is a very interesting case in molecular spectroscopy. For most molecular species, the line shape is greatly dominated by one, two, or sometimes three contributions, and others are either completely negligible or have a small impact. Here, we were able to properly interpret all the collisional contributions in the case when all six effects play an important role.

5. Conclusion

In this work, we used the highly accurate experimental spectra of the 3-0 S(1) and 2-0 Q(1) molecular hydrogen absorption lines perturbed by helium to study collisional line-shape effects. We clearly distinguished the influence of six different collisional effects (i.e.: collisional broadening and shift, their speed dependencies, and the complex Dicke effect) on the shapes of the H_2 lines. We showed that only the specific combination of these six contributions, obtained from our *ab initio* calculations, gives unprecedentedly good agreement with experimental spectra. If any one of the six contributions is neglected, then the agreement between the experiment and theory worsens at least several times. We also included the centrifugal distortion in our *ab initio* calculations, which further improved the agreement with the experimental spectra.

Declaration of Competing Interest

The authors declare that they have no known competing financial interests or personal relationships that could have appeared to influence the work reported in this paper.

CRediT authorship contribution statement

Michał Słowiński: Methodology, Software, Validation, Formal analysis, Investigation, Writing – original draft, Writing – review & editing, Visualization. **Hubert Jóźwiak:** Methodology, Software, Validation, Formal analysis, Investigation, Writing – original draft, Writing – review & editing, Visualization. **Maciej Gancewski:** Software, Validation, Investigation. **Kamil Stankiewicz:** Software, Validation, Investigation. **Nikodem Stolarczyk:** Methodology, Validation, Investigation, Writing – original draft, Writing – review & editing, Visualization. **Yan Tan:** Investigation. **Jin Wang:** Investigation. **An-Wen Liu:** Investigation. **Shui-Ming Hu:** Investigation. **Samir Kassi:** Investigation. **Alain Campargue:** Investigation. **Konrad Patkowski:** Software, Investigation, Writing – review & editing. **Piotr S. Żuchowski:** Software, Investigation. **Roman Ciuryło:** Conceptualization, Methodology. **Franck Thibault:** Conceptualization, Methodology, Software, Validation. **Piotr Wcisło:** Conceptualization, Methodology, Validation, Writing – original draft, Writing – review & editing, Project administration.

Acknowledgments

M.S., M.G. and K.S. contributions are supported by the *A next-generation worldwide quantum sensor network with optical atomic clocks* project carried out within the TEAM IV Programme of the Foundation for Polish Science cofinanced by the European Union under the European Regional Development Fund. P.W. and H.J. contributions are supported by the National Science Centre, Poland, Project No. 2018/31/B/ST2/00720. N.S. contribution is supported by the National Science Centre, Poland, Project No. 2019/35/B/ST2/01118. S.-M.H. acknowledges the support from National Natural Science Foundation of China (21688102). S.K. and A.C. acknowledge funding support from the Agence Nationale de la Recherche (Equipex REFIMEVE+ANR-11-EQPX-0039). K.P. is supported by the U.S. National Science Foundation award CHE-1955328. The project is cofinanced by the Polish National Agency for Academic Exchange under the PHC Polonium program (dec. PPN/X/PS/318/2018). The research is part of the program of the National Laboratory FAMO in Toruń, Poland. It is also supported by the COST Action CM1405 MOLIM.

Appendix A

In this Appendix we derive analytical formulas representing the relative root-mean-square error (rRMSE) for the small perturbation of the broadening and shift parameters. By this analysis one can quantify how an error on the line-shape parameters propagates on the final spectral line-shape-profile accuracy. We utilize a simple example of the normalized Lorentz profile

$$L(\omega;\Gamma,\Delta)=\frac{1}{\pi}\frac{\Gamma}{\Gamma^2+(\omega-\Delta)^2}. \tag{A.1}$$

Perturbation of the broadening parameter

We analyze a small change of the broadening parameter $\Gamma\rightarrow\Gamma+\epsilon\Gamma$. The relative difference caused by the perturbance of the profile is

$$D_\Gamma(\omega;\epsilon\Gamma)=\frac{L(\omega;\Gamma+\epsilon\Gamma,\Delta)-L(\omega;\Gamma,\Delta)}{L(0;\Gamma,\Delta)}. \tag{A.2}$$

To quantify the error on the final line-shape profile, we utilize rRMSE at $\pm$ FWHM of the line center, which can be expressed as

$$rRMSE(\epsilon\Gamma)=\sqrt{\frac{1}{4\Gamma}\int_{-2\Gamma}^{2\Gamma}[D_\Gamma(\omega;\epsilon\Gamma)]^2d\omega}. \tag{A.3}$$

Because $L(0;\Gamma,\Delta)$ is independent on ω, one can calculate typical RMSE and divide it by $L(0;\Gamma,\Delta)$ to determine rRMSE as well.

Since our goal is only to quantify the errors, the actual position of the line is irrelevant and the vertical axis can be adjusted so that $\Delta=0$, which simplifies the further formulas. The integration in Eq. (A.3) can be analytically performed and, since we consider small perturbations of the line-shape parameters, expanded into a series, the linear term of which is

$$rRMSE(\epsilon\Gamma)\approx\frac{\sqrt{\frac{73}{15}+\frac{25\mathrm{atan}2}{2}}}{10}\frac{\epsilon\Gamma}{\Gamma}\approx 0.433\frac{\epsilon\Gamma}{\Gamma}. \tag{A.4}$$

The above formula allows to estimate the rRMSE caused by the change $\epsilon\Gamma$ of broadening line-shape parameter, Γ.

Perturbation of the shift parameter

We repeat above discussion for the case of a small change of the shift parameter $\Delta\rightarrow\Delta+\epsilon\Delta$. The relative difference caused by the perturbance of the profile is

$$D_\Delta(\omega;\epsilon\Delta)=\frac{L(\omega;\Gamma,\Delta+\epsilon\Delta)-L(\omega;\Gamma,\Delta)}{L(0;\Gamma,\Delta)}. \tag{A.5}$$

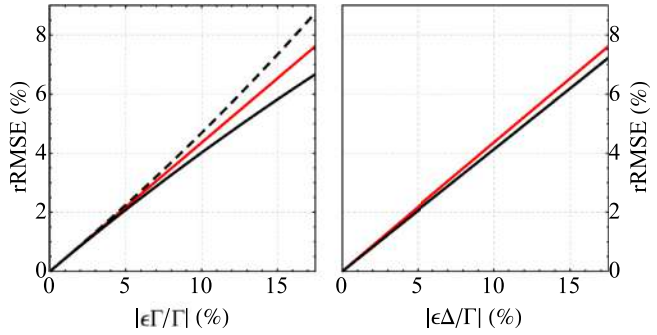

Fig. A1. The numerical validation of the analytical formulas for the relative root mean square errors (see text for more details). The black curves represent the numerical values and the red ones stand for analytical ones. Dashed and plain black curves of left panel corresponds to the negative and positive values of $\epsilon\Gamma/\Gamma$, respectively.

The same reason as mentioned before allows us to exclude Δ parameter and focus only on its distortion, i.e., $\epsilon\Delta$. Again, we quantify the error by calculating rRMSE at $\pm$FWHM, which is

$$rRMSE(\epsilon\Delta) = \sqrt{\frac{1}{4\Gamma}\int_{-2\Gamma}^{2\Gamma}[D_\Delta(\omega;\epsilon\Delta)]^2 d\omega}. \quad (A.6)$$

Similarly, rRMSE can be determined by dividing typically calculated RMSE by $L(0;\Gamma,\Delta)$. The integral can be analytically performed, expanded into series and since we consider small perturbations again, approximated by linear term which is

$$rRMSE(\epsilon\Delta) \approx \frac{\sqrt{\frac{77}{15}+\frac{25\text{atan}2}{2}}}{10}\frac{\epsilon\Delta}{\Gamma} \approx 0.436\frac{\epsilon\Delta}{\Gamma}. \quad (A.7)$$

The above formula allows to estimate the rRMSE caused by the change $\epsilon\Delta$ of shift line-shape parameter, Δ.

The direct comparison of the numerical results with Eqs. (A.4) and (A.7) is presented in Fig. A.1.

References

[1] Słowiński M, Thibault F, Tan Y, Wang J, Liu A-W, Hu S-M, Kassi S, Campargue A, Konefał M, Jóźwiak H, Patkowski K, Żuchowski P, Ciuryło R, Lisak D, Wcisło P. H_2-He collisions: *ab initio* theory meets cavity-enhanced spectra. Phys Rev A 2020;101(5):052705. doi:10.1103/physreva.101.052705.

[2] Bakr BW, Smith DGA, Patkowski K. Highly accurate potential energy surface for the He–H_2 dimer. J Chem Phys 2013;139(14):144305. doi:10.1063/1.4824299.

[3] Thibault F, Patkowski K, Żuchowski PS, Jóźwiak H, Ciuryło R, Wcisło P. Rovibrational line-shape parameters for H_2 in He and new H_2-He potential energy surface. J Quant Spectrosc Radiat Transf 2017;202:308–20. doi:10.1016/j.jqsrt.2017.08.014.

[4] Herzberg G, Howe LL. The Lyman bands of molecular hydrogen. Can J Phys 1959;37(5):636–59. doi:10.1139/p59-070.

[5] Thibault F, Wcisło P, Ciuryło R. A test of H_2-He potential energy surfaces. Eur Phys J D 2016;70(11):236. doi:10.1140/epjd/e2016-70114-9.

[6] Wcisło P, Gordon IE, Tran H, Tan Y, Hu S-M, Campargue A, Kassi S, Romanini D, Hill C, Kochanov RV, Rothman LS. The implementation of non-Voigt line profiles in the HITRAN database: H_2 case study. J Quant Spectrosc Radiat Transf 2016;177:75–91. doi:10.1016/j.jqsrt.2016.01.024.

[7] Perreault WE, Mukherjee N, Zare RN. Quantum control of molecular collisions at 1 kelvin. Science 2017;358(6361):356–9. doi:10.1126/science.aao3116.

[8] Perreault WE, Mukherjee N, Zare RN. Cold quantum-controlled rotationally inelastic scattering of HD with H_2 and D_2 reveals collisional partner reorientation. Nat Chem 2018;10(5):561–7. doi:10.1038/s41557-018-0028-5.

[9] Perreault WE, Mukherjee N, Zare RN. HD (v = 1, j = 2, m) orientation controls HD-He rotationally inelastic scattering near 1 K. J Chem Phys 2019;150(17):174301. doi:10.1063/1.5096531.

[10] Hout KVD, Hermans P, Mazur E, Knaap H. The broadening and shift of the rotational Raman lines for hydrogen isotopes at low temperatures. Physica A 1980;104(3):509–47. doi:10.1016/0378-4371(80)90012-6.

[11] Bragg SL, Smith WH, Brault JW. Line positions and strengths in the H_2 quadrupole spectrum. Astrophys J 1982;263:999. doi:10.1086/160568.

[12] Bischel WK, Dyer MJ. Temperature dependence of the Raman linewidth and line shift for the Q(1) and Q(0) transitions in normal and para–H_2. Phys Rev A 1986;33(5):3113–23. doi:10.1103/physreva.33.3113.

[13] Rahn LA, Rosasco GJ. Measurement of the density shift of the H_2 Q(0–5) transitions from 295 to 1000 K. Phys Rev A 1990;41(7):3698–706. doi:10.1103/physreva.41.3698.

[14] Rahn LA, Farrow RL, Rosasco GJ. Measurement of the self-broadening of the H_2 Q(0–5) Raman transitions from 295 to 1000 K. Phys Rev A 1991;43(11):6075–88. doi:10.1103/physreva.43.6075.

[15] Forsman JW, Bonamy J, Robert D, Berger JP, Saint-Loup R, Berger H. H_2-He vibrational line-shape parameters: measurement and semiclassical calculation. Phys Rev A 1995;52(4):2652–63. doi:10.1103/physreva.52.2652.

[16] Sinclair PM, Berger JP, Michaut X, Saint-Loup R, Chaux R, Berger H, Bonamy J, Robert D. Collisional broadening and shifting parameters of the Raman Q branch of H_2 perturbed by N_2 determined from speed-dependent line profiles at high temperatures. Phys Rev A 1996;54(1):402–9. doi:10.1103/physreva.54.402.

[17] Wcisło P, Thibault F, Stolarczyk N, Jóźwiak H, Słowiński M, Gancewski M, Stankiewicz K, Konefał M, Kassi S, Campargue A, Tan Y, Wang J, Patkowski K, Ciuryło R, Lisak D, Kochanov R, Rothman L, Gordon I. The first comprehensive dataset of beyond-Voigt line-shape parameters from ab initio quantum scattering calculations for the HITRAN database: He-perturbed H_2 case study. J Quant Spectrosc Radiat Transf 2021;260:107477. doi:10.1016/j.jqsrt.2020.107477.

[18] Hermans P, Die AV, Knaap H, Beenakker J. Measurements on the influence of binary collisions on the depolarized Rayleigh and rotational Raman lines for H_2-noble gas systems at low temperatures. Physica A 1985;132(2–3):233–52. doi:10.1016/0378-4371(85)90010-x.

[19] Blackmore R, Green S, Monchick L. Dicke narrowing of the polarized Stokes–Raman Q branch of the v=0→1 transition of D_2 in He. J Chem Phys 1989;91(7):3846–53. doi:10.1063/1.457640.

[20] Michaut X, Saint-Loup R, Berger H, Dubernet ML, Joubert P, Bonamy J. Investigations of pure rotational transitions of H_2 self-perturbed and perturbed by He. I. Measurement, modeling, and quantum calculations. J Chem Phys 1998;109(3):951–61. doi:10.1063/1.476638.

[21] Martínez RZ, Bermejo D, Thibault F, Wcisło P. Testing the ab initio quantum-scattering calculations for the D_2-He benchmark system with stimulated Raman spectroscopy. J Raman Spectrosc 2018;49(8):1339–49. doi:10.1002/jrs.5391.

[22] Jóźwiak H, Thibault F, Stolarczyk N, Wcisło P. Ab initio line-shape calculations for the S and O branches of H_2 perturbed by He. J Quant Spectrosc Radiat Transf 2018;219:313–22. doi:10.1016/j.jqsrt.2018.08.023.

[23] Thibault F, Martínez RZ, Bermejo D, Wcisło P. Line-shape parameters for the first rotational lines of HD in He. Mol Astrophys 2020;19:100063. doi:10.1016/j.molap.2020.100063.

[24] Morita M, Balakrishnan N. Stereodynamics of rotationally inelastic scattering in cold He+HD collisions. J Chem Phys 2020a;153(9):091101. doi:10.1063/5.0022190.

[25] Morita M, Balakrishnan N. Stereodynamics of ultracold rotationally inelastic collisions. J Chem Phys 2020b;153(18):184307. doi:10.1063/5.0030808.

[26] Stankiewicz K, Jóźwiak H, Gancewski M, Stolarczyk N, Thibault F, Wcisło P. Ab initio calculations of collisional line–shape parameters and generalized spectroscopic cross-sections for rovibrational dipole lines in HD perturbed by He. J Quant Spectrosc Radiat Transf 2020;254:107194. doi:10.1016/j.jqsrt.2020.107194.

[27] Komasa J, Piszczatowski K, Łach G, Przybytek M, Jeziorski B, Pachucki K. Quantum electrodynamics effects in rovibrational spectra of molecular hydrogen. J Chem Theory Comput 2011;7(10):3105–15. doi:10.1021/ct200438t.

[28] Feuchtgruber H, Lellouch E, Bézard B, Encrenaz T, de Graauw T, Davis GR. Detection of HD in the atmospheres of Uranus and Neptune: a new determination of the D/H ratio. Astron Astrophys 1999;341:L17–21. https://ui.adsabs.harvard.edu/abs/1999A&A...341L..17F

[29] Lellouch E, Bézard B, Fouchet T, Feuchtgruber H, Encrenaz T, de Graauw T. The deuterium abundance in Jupiter and Saturn from ISO-SWS observations. Astron Astrophys 2001;370(2):610–22. doi:10.1051/0004-6361:20010259.

[30] Lellouch E, Hartogh P, Feuchtgruber H, Vandenbussche B, de Graauw T, Moreno R, Jarchow C, Cavalié T, Orton G, Banaszkiewicz M, Blecka MI, Bockelée-Morvan D, Crovisier J, Encrenaz T, Fulton T, Küppers M, Lara LM, Lis DC, Medvedev AS, Rengel M, Sagawa H, Swinyard B, Szutowicz S, Bensch F, Bergin E, Billebaud F, Biver N, Blake GA, Blommaert JADL, Cernicharo J, Courtin R, Davis GR, Decin L, Encrenaz P, Gonzalez A, Jehin E, Kidger M, Naylor D, Portyankina G, Schieder R, Sidher S, Thomas N, de Val-Borro M, Verdugo E, Waelkens C, Walker H, Aarts H, Comito C, Kawamura JH, Maestrini A, Peacocke T, Teipen R, Tils T, Wildeman K. First results of Herschel-PACS observations of Neptune. Astron Astrophys 2010;518:L152. doi:10.1051/0004-6361/201014600.

[31] Feuchtgruber H, Lellouch E, Orton G, de Graauw T, Vandenbussche B, Swinyard B, Moreno R, Jarchow C, Billebaud F, Cavalié T, Sidher S, Hartogh P. The D/H ratio in the atmospheres of Uranus and Neptune from Herschel-PACS observations. Astron Astrophys 2013;551:A126. doi:10.1051/0004-6361/201220857.

[32] Smith WH. The H_2 4-0 S(0, 1,and 2) quadrupole features in Jupiter. Icarus 1989;81(2):429–40. doi:10.1016/0019-1035(89)90062-6.

[33] Baines KH, Mickelson ME, Larson LE, Ferguson DW. The abundances of methane and ortho/para hydrogen on Uranus and Neptune: implications of new laboratory 4-0 h_2 quadrupole line parameters. Icarus 1995;114(2):328–40. doi:10.1006/icar.1995.1065.

[34] Ciuryło R, Shapiro DA, Drummond JR, May AD. Solving the line-shape problem with speed-dependent broadening and shifting and with Dicke narrowing. II. Application. Phys Rev A 2002a;65(1):012502. doi:10.1103/physreva.65.012502.

[35] Wcisło P, Thibault F, Zaborowski M, Wójtewicz S, Cygan A, Kowzan G, Masłowski P, Komasa J, Puchalski M, Pachucki K, Ciuryło R, Lisak D. Accu-

rate deuterium spectroscopy for fundamental studies. J Quant Spectrosc Radiat Transf 2018;213:41–51. doi:10.1016/j.jqsrt.2018.04.011.
[36] Ciuryło R, Bielski A, Drummond JR, Lisak D, May AD, Pine AS, Shapiro DA, Szudy J, Trawiński RS. High-resolution studies on the influence of velocity-changing collisions on atomic and molecular line shapes. AIP Conf Proc, AIP 2002b. doi:10.1063/1.1525447.
[37] Lisak D, Hodges J, Ciuryło R. Comparison of semiclassical line-shape models to rovibrational H_2O spectra measured by frequency-stabilized cavity ring-down spectroscopy. Phys Rev A 2006;73(1):012507. doi:10.1103/physreva.73.012507.
[38] Hess S. Kinetic theory of spectral line shapes. The transition between doppler broadening and collisional broadening. Physica 1972;61(1):80–94. doi:10.1016/0031-8914(72)90035-3.
[39] Corey GC, McCourt FR. Dicke narrowing and collisional broadening of spectral lines in dilute molecular gases. J Chem Phys 1984;81(5):2318–29. doi:10.1063/1.447930.
[40] Monchick L, Hunter LW. Diatomic–diatomic molecular collision integrals for pressure broadening and Dicke narrowing: a generalization of Hess's theory. J Chem Phys 1986;85(2):713–18. doi:10.1063/1.451277.
[41] Berman PR. Speed-dependent collisional width and shift parameters in spectral profiles. J Quant Spectrosc Radiat Transf 1972;12(9):1331–42. doi:10.1016/0022-4073(72)90189-6.
[42] Pickett HM. Effects of velocity averaging on the shapes of absorption lines. J Chem Phys 1980;73(12):6090–4. doi:10.1063/1.440145.
[43] Pine A. Asymmetries and correlations in speed-dependent Dicke-narrowed line shapes of argon-broadened HF. J Quant Spectrosc Radiat Transf 1999;62(4):397–423. doi:10.1016/s0022-4073(98)00112-5.
[44] Rautian SG, Sobelman II. The effect of collisions on the Doppler broadening of spectral lines. Sov Phys Usp 1967;9(5):701–16. doi:10.1070/pu1967v009n05abeh003212.
[45] Demeio L, Green S, Monchick L. Effects of velocity changing collisions on line shapes of HF in Ar. J Chem Phys 1995;102(23):9160–6. doi:10.1063/1.468864.
[46] Schaefer J, Monchick L. Line broadening of HD immersed in He and H_2 gas. Astron Astrophys 1992;265(2):859–68. doi:10.1063/1.453612.
[47] Stolarczyk N, Thibault F, Cybulski H, Jóźwiak H, Kowzan G, Vispoel B, Gordon I, Rothman L, Gamache R, Wcisło P. Evaluation of different parameterizations of temperature dependences of the line-shape parameters based on ab initio calculations: case study for the HITRAN database. J Quant Spectrosc Radiat Transf 2020;240:106676. doi:10.1016/j.jqsrt.2019.106676.
[48] Kowzan G, Wcisło P, Słowiński M, Masłowski P, Viel A, Thibault F. Fully quantum calculations of the line-shape parameters for the Hartmann-Tran profile: A CO-Ar case study. J Quant Spectrosc Radiat Transf 2020;243:106803. doi:10.1016/j.jqsrt.2019.106803.
[49] Shafer R, Gordon RG. Quantum scattering theory of rotational relaxation and spectral line shapes in H_2–He gas mixtures. J Chem Phys 1973;58(12):5422–43. doi:10.1063/1.1679162.
[50] Ben-Reuven A. Symmetry considerations in pressure-broadening theory. Phys Rev 1966a;141(1):34–40. doi:10.1103/PhysRev.141.34.
[51] Ben-Reuven A. Impact broadening of microwave spectra. Phys Rev 1966b;145(1):7–22. doi:10.1103/PhysRev.145.7.
[52] Schaefer J, Monchick L. Line shape cross sections of HD immersed in HE and H_2 gas. I. Pressure broadening cross sections. J Chem Phys 1987;87(1):171–81. doi:10.1063/1.453612.
[53] Shapiro DA, Ciuryło R, Drummond JR, May AD. Solving the line-shape problem with speed-dependent broadening and shifting and with Dicke narrowing. I. Formalism. Phys Rev A 2002;65(1):012501. doi:10.1103/physreva.65.012501.
[54] Blackmore R. A modified Boltzmann kinetic equation for line shape functions. J Chem Phys 1987;87(2):791–800. doi:10.1063/1.453286.
[55] Smith EW, Cooper J, Chappell W, Dillon T. An impact theory for Doppler and pressure broadening II. Atomic and molecular systems. J Quant Spectrosc Radiat Transf 1971;11(10):1567–76. doi:10.1016/0022-4073(71)90114-2.
[56] Nienhuis G. Effects of the radiator motion in the classical and quantum-mechanical theories of collisional spectral-line broadening. J Quant Spectrosc Radiat Transf 1978;20(3):275–90. doi:10.1016/0022-4073(78)90133-4.
[57] Lindenfeld MJ. Self-structure factor of hard-sphere gases for arbitrary ratio of bath to test particle masses. J Chem Phys 1980;73(11):5817–29. doi:10.1063/1.440066.
[58] Liao PF, Bjorkholm JE, Berman PR. Effects of velocity-changing collisions on two-photon and stepwise-absorption spectroscopic line shapes. Phys Rev A 1980;21(6):1927–38. doi:10.1103/physreva.21.1927.
[59] Nelkin M, Ghatak A. Simple binary collision model for Van Hove's $G_s(r,t)$. Phys Rev 1964;135(1A):A4–9. doi:10.1103/PhysRev.135.A4.
[60] Wcisło P, Tran H, Kassi S, Campargue A, Thibault F, Ciuryło R. Velocity-changing collisions in pure H_2 and H_2-Ar mixture. J Chem Phys 2014;141(7):074301. doi:10.1063/1.4892414.
[61] Chapman S, Cowling TG. The mathematical theory of non-Uniform gases. Cambridge University Press; 1970.
[62] Hirshfelder JO, Curtiss CF, Bird RB. Nonequilibrium phenomena in polyatomic gases. Wiley; 1954.
[63] Taylor WL, Hurly JJ, Meyer BA, Dunlop PJ. Binary diffusion coefficients of helium/hydrogen isotope mixtures. J Chem Phys 1995;103(16):6959–65. doi:10.1063/1.470373.
[64] Jóźwiak H., Gancewski M., Grabowski A., Stankiewicz K., Wcisło P.. BIGOS computer code, to be published.
[65] Benner DC, Rinsland CP, Devi VM, Smith MAH, Atkins D. A multispectrum nonlinear least squares fitting technique. J Quant Spectrosc Radiat Transf 1995;53(6):705–21. doi:10.1016/0022-4073(95)00015-d.
[66] Humlíček J. An efficient method for evaluation of the complex probability function: The Voigt function and its derivatives. J Quant Spectrosc Radiat Transf 1979;21(4):309–13. doi:10.1016/0022-4073(79)90062-1.
[67] Schreier F. Optimized implementations of rational approximations for the Voigt and complex error function. J Quant Spectrosc Radiat Transf 2011;112(6):1010–25. doi:10.1016/j.jqsrt.2010.12.010.
[68] Duggan P, Sinclair P, Berman R, May A, Drummond JR. Testing lineshape models: measurements for v = 1–0 CO broadened by He and Ar. J Mol Spectrosc 1997;186(1):90–8. doi:10.1006/jmsp.1997.7420.
[69] Ngo N, Lisak D, Tran H, Hartmann JM. An isolated line-shape model to go beyond the Voigt profile in spectroscopic databases and radiative transfer codes. J Quant Spectrosc Radiat Transf 2013;129:89–100. doi:10.1016/j.jqsrt.2013.05.034.
[70] Wcisło P, Thibault F, Cybulski H, Ciuryło R. Strong competition between velocity-changing and phase- or state-changing collisions in H_2 spectra perturbed by Ar. Phys Rev A 2015;91(5):052505. doi:10.1103/physreva.91.052505.
[71] Farrow RL, Rahn LA, Sitz GO, Rosasco GJ. Observation of a speed-dependent collisional inhomogeneity in H_2 vibrational line profiles. Phys Rev Lett 1989;63(7):746–9. doi:10.1103/physrevlett.63.746.
[72] Joubert P, Bonamy J, Robert D, Domenech J-L, Bermejo D. A partially correlated strong collision model for velocity- and state-changing collisions. Application to Ar-broadened HF rovibrational line shape. J Quant Spectrosc Radiat Transf 1999;61(4):519–31. doi:10.1016/s0022-4073(98)00038-7.
[73] Ciuryło R, Pine A, Szudy J. A generalized speed-dependent line profile combining soft and hard partially correlated Dicke-narrowing collisions. J Quant Spectrosc Radiat Transf 2001;68(3):257–71. doi:10.1016/s0022-4073(00)00024-8.
[74] Lisak D, Rusciano G, Sasso A. Speed-dependent and correlation effects on the line shape of acetylene. Phys Rev A 2005;72(1):012503. doi:10.1103/physreva.72.012503.
[75] Lisak D, Cygan A, Bermejo D, Domenech J, Hodges J, Tran H. Application of the Hartmann–Tran profile to analysis of H_2O spectra. J Quant Spectrosc Radiat Transf 2015;164:221–30. doi:10.1016/j.jqsrt.2015.06.012.
[76] Marteau P, Boulet C, Robert D. Finite duration of collisions and vibrational dephasing effects on the Ar broadened HF infrared line shapes: asymmetric profiles. J Chem Phys 1984;80(8):3632–9. doi:10.1063/1.447184.
[77] Sheldon G, Sinclair P, Flohic ML, Drummond J, May A. Line mixing and broadening in the Raman Q branch of HD at 304.6 K. J Mol Spectrosc 1998;192(2):406–16. doi:10.1006/jmsp.1998.7696.
[78] Schaefer J, Köhler W. Quantum calculations of rotational and NMR relaxation, depolarized Rayleigh and rotational Raman line shapes for H_2(HD)-He mixtures. Physica A 1985;129(3):469–502. doi:10.1016/0378-4371(85)90181-5.
[79] Muchnick P, Russek A. The HeH_2 energy surface. J Chem Phys 1994;100(6):4336–46. doi:10.1063/1.466316.
[80] Boothroyd AI, Martin PG, Peterson MR. Accurate analytic He–H_2 potential energy surface from a greatly expanded set of ab initio energies. J Chem Phys 2003;119(6):3187–207. doi:10.1063/1.1589734.
[81] Meyer W, Hariharan PC, Kutzelnigg W. Refined ab initio calculation of the potential energy surface of the He–H_2 interaction with special emphasis to the region of the van der Waals minimum. J Chem Phys 1980;73(4):1880–97. doi:10.1063/1.440324.
[82] Tao FM. An accurate ab initio potential energy surface of the He–H_2 interaction. J Chem Phys 1994;100(7):4947–54. doi:10.1063/1.467214.
[83] Campargue A, Kassi S, Pachucki K, Komasa J. The absorption spectrum of H_2: CRDS measurements of the (2-0) band, review of the literature data and accurate ab initio line list up to 35000 cm^{-1}. Phys Chem Chem Phys 2012;14(2):802–15. doi:10.1039/c1cp22912e.
[84] Green S, Blackmore R, Monchick L. Comment on linewidths and shifts in the Stokes–Raman Q branch of D_2 in He. J Chem Phys 1989;91(1):52–5. doi:10.1063/1.457489.
[85] Dubernet M-L, Tuckey P. Raman Q and S line broadening and shifting coefficients: some commonly used assumptions revisited. Chem Phys Lett 1999;300(3–4):275–80. doi:10.1016/s0009-2614(98)01334-7.
[86] Mondelain D, Kassi S, Campargue A. Transition frequencies in the (2-0) band of D2 with MHz accuracy. J Quant Spectrosc Radiat Transf 2020;253:107020. doi:10.1016/j.jqsrt.2020.107020.